Prediction of the aerodynamic performance of the Mexico rotor by using airfoil data extracted from CFD

Yang, Hua; Shen, Wen Zhong; Xu, Haoran; Hong, Zedong; Liu, Chao

Published in:
Proceedings of the 2013 International Conference on aerodynamics of Offshore Wind Energy Systems and wakes (ICOWES2013)

Publication date:
2013

Document Version
Publisher's PDF, also known as Version of record

PREDICTION OF THE AERODYNAMIC PERFORMANCE OF THE MEXICO ROTOR BY USING AIRFOIL DATA EXTRACTED FROM CFD

Hua Yang[1], Wenzhong Shen[2], Haoran Xu[3], Zedong Hong[1], Chao Liu[3]

[1]College of Power and Energy Engineering, Yangzhou University, Yangzhou, China, yanghua@yzu.edu.cn
[2]Department of Wind Energy, Technical University of Denmark, DK-2800 Lyngby, Denmark, wzsh@dtu.dk
[3]College of Water Conservancy Science and Engineering, Yangzhou University, Yangzhou, China, ydxuhaoran@163.com

ABSTRACT

Blade Element Momentum (BEM) theory is a widely used technique for prediction of wind turbine aerodynamics performance, but the reliability of airfoil data is an important factor to improve the prediction accuracy of aerodynamic loads and power using a BEM code. The airfoil characteristics used in BEM codes are mostly based on 2D wind tunnel measurements of airfoils with constant span. However, a BEM code using airfoil data obtained directly from 2D wind tunnel measurements will not yield the correct loading and power. As a consequence, 2D airfoil characteristics have to be corrected by using some models before they can be used in a BEM code. In this article, the airfoil data for the MEXICO (Model EXperiments in Controlled cOnditions) rotor are extracted from CFD (Computational Fluid Dynamics) results. The azimuthally averaged velocity is used as the sectional velocity to define the angle of attack and the coefficient of lift and drag is determined by the forces on the blade. The extracted airfoil data are put into a BEM code without corrections of rotational or tip effects, and the calculated axial and tangential forces are compared to both computations using BEM with Shen's tip loss correction models and experimental data. The comparisons show that the present method of determination of angle of attack is correct, and the re-calculated forces have good agreements with the experiment.

Key words: wind turbine, rotor aerodynamics, airfoil data

1 Introduction

BEM (Blade Element Momentum) theory is widely used to perform the aerodynamic prediction of horizontal axis wind turbines due to the requirement of less computational time. The load prediction accuracy of BEM depends on the reliability of the data of airfoil characteristics[1]. When wind turbine blade is rotating, the centrifugal force drives the air in the boundary layer flow to the blade tip. The Coriolis force produces an additional pressure gradient along the chordwise direction and drives the air flow to the trailing edge of the blade. All these make the boundary layer become thinner and the separation point of flow moves close to the trailing edge. So the stall angle of attack of airfoil at rotating condition is larger than at static condition, this phenomenon is so called stall delay. Because of the differences between the aerodynamic characteristics of blade in rotating and static condition, the two-dimensional airfoil characteristic data cannot be directly used in BEM to predict the performance of a rotating blade, and aerodynamic correction should be made for two-dimensional airfoil characteristic data. Some scholars have performed some research work on the correction for airfoil data by using of theoretical analysis and experiment. Various models have been developed by e.g. Snel *et al*.,[2] Du and Selig,[3] Chaviaropoulos and Hansen.[4] The airfoil characteristics can also be derived from experimental velocity and pressure data.[5]

With the development of computational technique, CFD (Computational Fluid Dynamics) method is widely used to perform research on predicting aerodynamic performance of wind turbines and developing new airfoils. Although CFD method takes a long time for calculation and has high requirement on computer hardware, CFD plays an important role on displaying detailed structure of flow (checking up and estimating the region of flow separation) and validating the empirical calculation model. Airfoil data can also be extracted directly from CFD rotor computations.[6]

In this article, CFD method is applied to perform numerical simulation on the MEXICO (Model EXperiments In Controlled cOnditions) rotor at three operational wind speeds. The data of airfoil characteristics extracted from the calculated result are applied in BEM to predict the performance of MEXICO rotor under other operational conditions, and the result calculated by BEM will be compared with experimental data to validate the prediction accuracy of CFD.

2 MEXICO rotor

The MEXICO project[7] was funded by the European Commission under FP5. The main objective was to create a database of detailed aerodynamic measurements on a wind turbine model to be used for model validation and improvement. The experiment was carried out at the Large Scale Low Speed Facility (LLF) of DNW German-Dutch wind tunnels, which is a high quality wind tunnel with a 9.5x9.5 m^2 open test section.

The rotor model has three blades with a diameter of 4.5 m. Three different airfoil sections were used in the design, DU91-W2-250 from 20% to 45% span, RISOE-A1-21 from 55% to 65% span and NACA 64-418 from 70% to 100% span. 148 dynamic pressured sensors were installed at five sections of 25%, 35%, 60%, 82% and 92% span to measure the blade surface pressure. Besides the pressure measurements, flow fields were also investigated by stereo PIV.

In the MEXICO experiment, various loads were measured using strain gauge techniques. These include the blade root flap moment, the edge moment and the low-speed shaft torque. Further details regarding the experiment can be found in Schepers *et al*.[7] The turbine was tested about 944 operational conditions, most of them under axial inflow conditions. Table 1 shows the operational axial-inflow conditions of the 9 cases used in the present study.

Table 1. Operational conditions used in the present study

Case number	Data file	Air density (kg m^{-3})	Wind speed (m s^{-1})	Rotational speed (rpm)	Tip speed ratio	Pitch angle (deg)
1	R011P0011D000111	1.188	10.00	423.5	10.0	0.7
2	R011P0011D000115	1.189	18.10	424.3	5.5	0.7
3	R011P0011D000117	1.188	24.00	424.4	4.2	0.7
4	R011P0011D000093	1.192	14.93	423.6	6.7	-2.3
5	R011P0011D000094	1.191	18.05	429.0	5.6	-2.3
6	R011P0011D000104	1.190	11.04	424.5	9.1	-2.3
7	R011P0011D000114	1.189	14.91	423.5	6.7	-5.3
8	R011P0011D000124	1.188	10.00	429.6	10.1	1.7
9	R011P0011D000127	1.188	14.96	424.4	6.7	-1.3

3 Numerical simulation

3.1 Numerical method

Steady numerical simulation method is employed to calculate the flow field of one blade passage under non-yawed condition. The size of the computational domain is shown in Figure 1(a). The inlet boundary is located at 4 times blade radius upstream and the outlet is located at 8 times bade radius downstream. The radius of computational domain is 4 times blade radius. The software of ICEM is used to generate the computational grid, the stationary domain is discretized by an unstructured tetrahedral mesh and the rotating domain is discretized by a structured hexahedral mesh. There are 3.6 $\times 10^6$ mesh elements in the one-third calculated domain as is shown in Figure 1(b). The hight of the first floor mesh element is about 3.6×10^{-5} m, which assures that y^+ is below 5 on the blade surface.

According to reference 8, the turbulence is modeled using Menter's *k-ω* SST turbulence model, which have the advantages of both $k-\omega$ and $k-\varepsilon$ models. At the same time, the cross-flow dissipation derivative integral is added into SST model, and the transport process of turbulence shear stress is taken into consideration in the definition of turbulent viscosity. So the SST model is more accurate of predicting the area of flow separation caused by adverse pressure gradient. SIMPLE algorithm is adopted to solve the full three-dimensional steady Reynolds time-averaged Navier-Stokes equations, and the convection terms are discretized with the second order upwind scheme.

Boundary conditions are as follows: prescribed axial velocity and static temperature at inlet; prescribed static pressure at outlet; non-slip flow is used on the surface of hub and blade; opening boundary conditions and circumferential periodic boundaries are used on outface and side surface respectively; the frozen technique is applied to dealing with the interface of rotational and stationary domains.

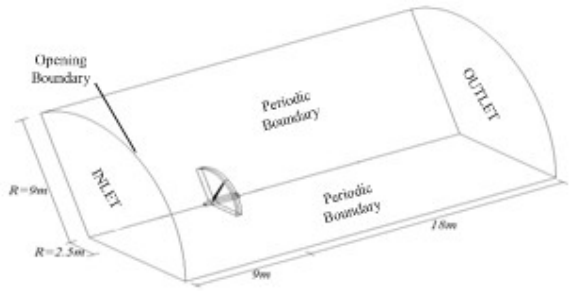

(a)

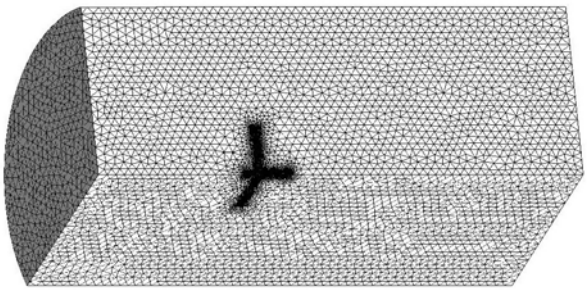

(b)

Fig. 1: Computational domain and mesh generation

3.2 Numerical simulation results

Numerical simulations are performed for case 1, 2, 3 in table 1. The distribution of pressure coefficient C_p at 60% span under three operating conditions is shown in Figure 2. From the figure it can be seen that the calculated C_p agrees well with experimental results when the tunnel velocity V_{tun} equals to 10 m/s and 18.1 m/s. When V_{tun} = 24 m/s, the calculated C_p on the pressure side agrees well with experimental results, while the C_p on the suction side is lower than experimental data, some pressure deviations exist between calculation and measurements, which may be caused by flow separation on the suction side. The limiting stream lines on the suction side are given in Figure 3. The figure shows that flow separation occurs at 60% span when the tunnel velocity is 24 m/s, while flow separation doesn't occur at the same blade when the inflow velocity is 10 m/s and 18.1 m/s. The separation flow area is increased with the increase of tunnel speed. The axial and tangential force can be calculated from the sectional pressure distribution. The comparison of axial and tangential force between calculations and measurements is shown in Figure 4. The figure indicates that the calculated force agrees well with the measured data. The axial force on the blade increases from hub to tip, while the

tangential force changes slightly along the radial direction. With the increase of tunnel velocity, the axial and tangential force at the same span increases.

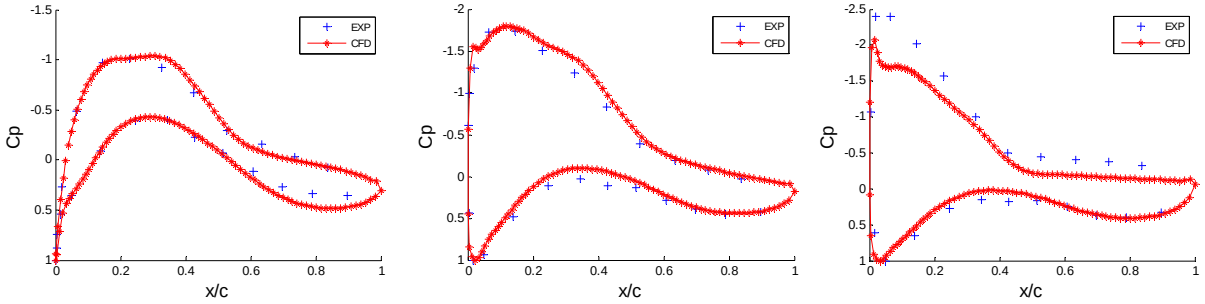

(a) V_{tun}=10m/s (b) V_{tun}= 18.1m/s (c) V_{tun}= 24m/s

Fig. 2: Pressure distributions at 60% span of the MEXICO blades threat the tunnel speeds of 10, 15 and 24 m/s.

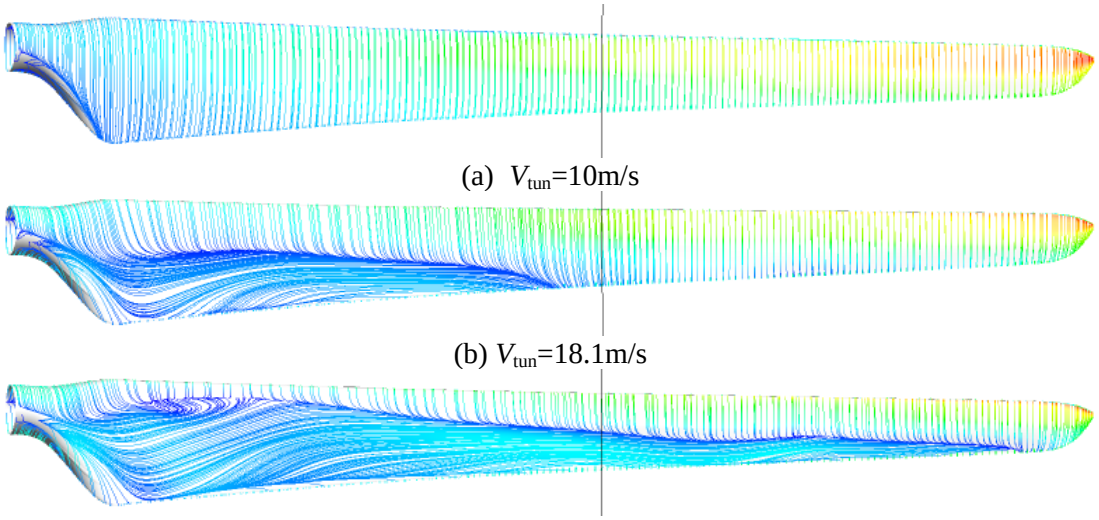

(a) V_{tun}=10m/s

(b) V_{tun}=18.1m/s

（c）V_{tun}=24m/s

Fig. 3: Limiting stream lines on the suction side of the MEXICO blades

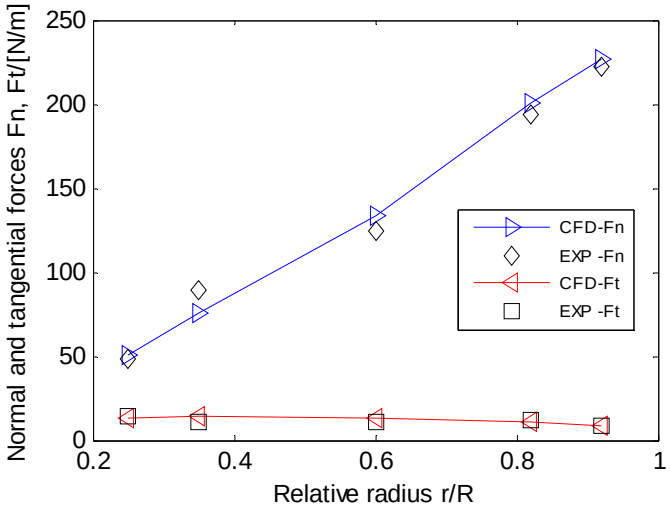

(a) V_{tun}= 10m/s

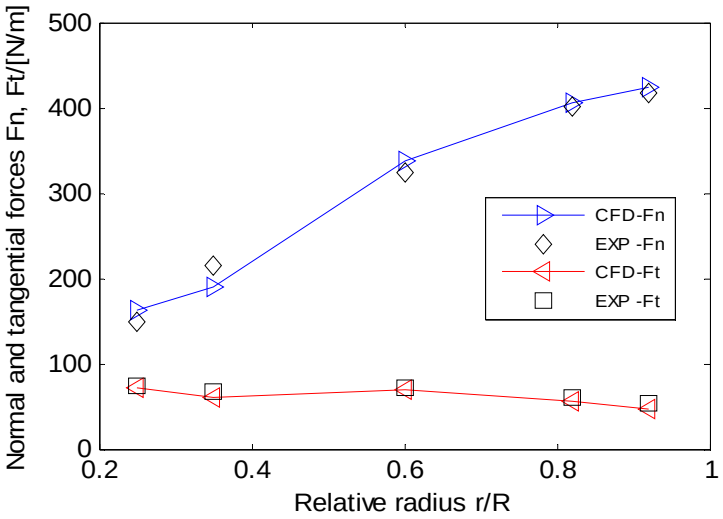

(b) V_{tun}=18.1m/s

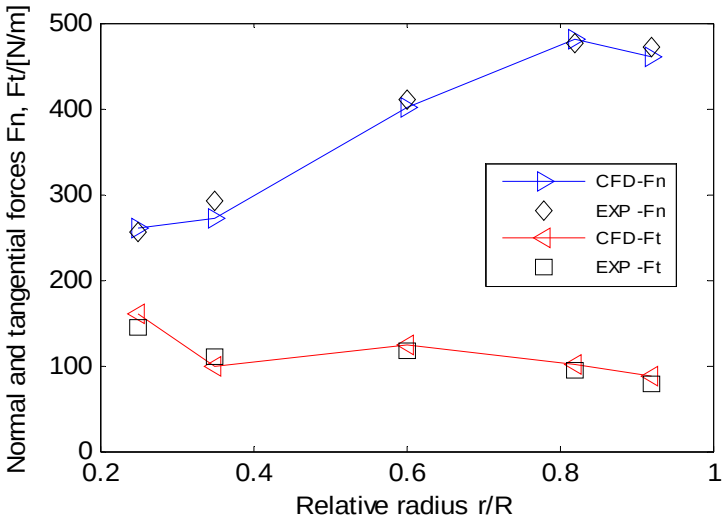

(c) V_{tun}= 24m/s

Fig. 4: Comparison of axial and tangential force distributions between experimental results and CFD results

4 Extraction of airfoil characteristics

4.1 Determination of the angle of attack

Because of the effect of centrifugal force and Coriolis force on the rotating blades, the airfoil characteristics have larger deviations between the static two-dimensional airfoil and the rotating three-dimensional airfoil. The flow field at the root part of blade is more complex, the two-dimensional airfoil data cannot be used by BEM directly and it should be corrected before it is used. In this article, the airfoil characteristics at the span of 25%, 35%, 55%, 60%, 65%, 75%, 82%, 85%, 92% is extracted from the numerical results.

The averaged azimuthally axial velocity V_{za} and tangential velocity V_{ta} on every section is calculated from the monitor points, shown in Figure 5, which are located in the circumferential direction every five degrees and in the rotating plane at a distance of one chord-length away from the leading edge. At last the relative velocity of a profile can be calculated according to the formula

$V_{rel} = \sqrt{V_{za}^2 + V_{ta}^2}$. As shown in Figure 6, the inflow angle can be defined as $\phi = \tan^{-1} \frac{V_{za}}{\Omega r + V_{ta}}$, and the angle of attack can be expressed as: $\alpha = \phi - \beta$, β can be determined according to the pitch angle and twist angle. The distribution of local pitch angle along the radial direction is given in Figure 7.

The distribution of angle of attack along the radial direction under three operating conditions is shown in Figure 8. It is obvious that, when the inflow velocity equals to 10 m/s, the angle of attack in the middle part is lower than that in the root and tip part of the blade. When the inflow velocity is equal to 18.1 m/s and 24 m/s, the angle of attack decreases monotone from the hub to the tip. Generally speaking, the variation amplitude of angle of attack under low inflow velocity is smaller than that under high inflow velocity.

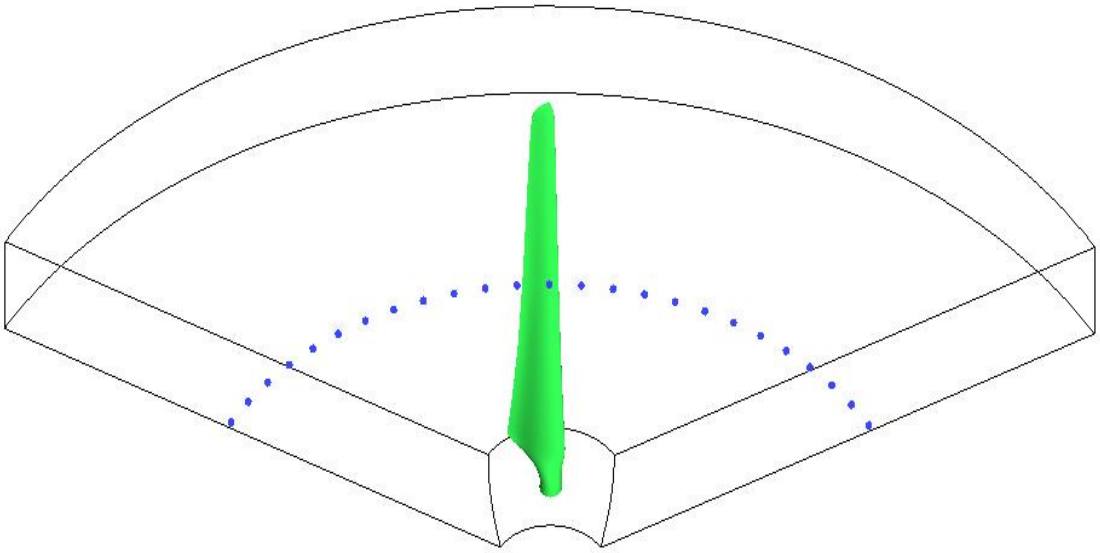

Fig. 5: Points for extraction velocity

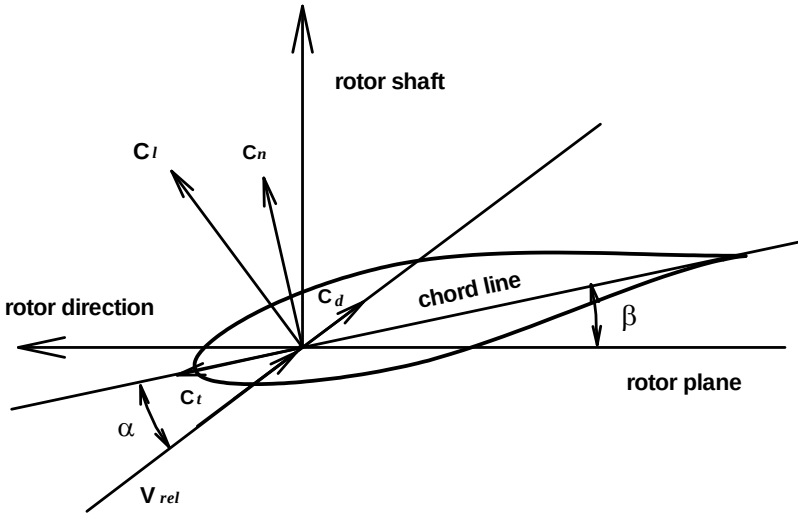

Fig. 6: Cross-section aerofoil element

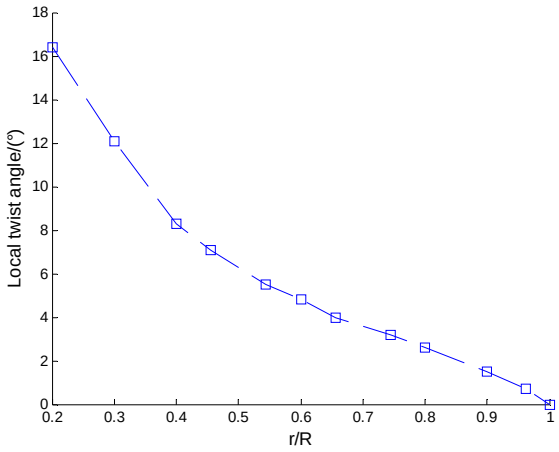

Fig. 7: Local twist angle along blade

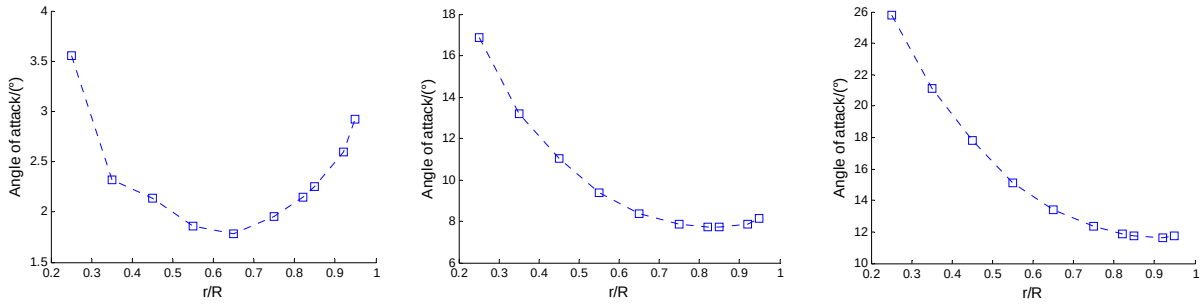

Fig. 8: Exacted angle of attack from CFD at three tunnel flow conditions

4.2 Determination of the lift and drag coefficient

From Figure 6, the local tangential force $C_t = \frac{F_t}{½\rho c V_{rel}^2}$ and normal force $C_n = \frac{F_n}{½\rho c V_{rel}^2}$ can be obtained from the computational pressure. When the local angle of attack and relative velocity are known, the lift and drag coefficients are calculated by formulae (1) and (2).

$$C_l = C_n \cos\alpha + C_t \sin\alpha \quad (1)$$

$$C_d = C_n \sin\alpha - C_t \cos\alpha \quad (2)$$

Where, ρ is the density of air, V_{rel} is the local velocity, c is chord length and α denotes the angle of attack.

4.3 Sectional airfoil characteristics

Three wind speeds are used to derive the airfoil characteristics in the present study, and the sectional airfoil data are fitted using spline interpolation functions. For comparison, 2D lift and drag coefficients are also plotted in Figure 9.

For the DU airfoil at the span of 25% and 35%, the stall angle of attack in the 2D case is about 10 degrees, which are less than the value of the rotating case. This phenomenon is called stall delay. When the angle of attack is less than 10 degrees, air is attached to the airfoil surface, the lift coefficient of the DU airfoil at both 25% and 35% span of the rotating blades is less than that in the 2D case and they are close to each other at the two spans. When the angle of attack is larger than 10 degrees, the lift coefficient of the DU airfoil at 25% span is larger than that in the 2D case, while at 35% span it is less than that of the 2D case. For the Risø airfoil at 55%, 60% and 65% span of the blades, the derived lift coefficient values are close to each other and less than that of the 2D case. With the increase of radius, the lift coefficient of the NACA airfoil in the outer part of blade decreases gradually.

The derived drag coefficient of the rotating DU airfoil is larger than that of the 2D case under the condition of both high and low angle of attack, while it is less than the 2D drag coefficient when the angle of attack is close to 15 degrees. For the Risø airfoil, the drag coefficient of 3D airfoil is less than

that of 2D airfoil. For the NACA airfoil, the 3D drag coefficient is larger than that of the 2D airfoil at high angle of attack, while the derived drag coefficient is less than that of the 2D airfoil at low angle of attack.

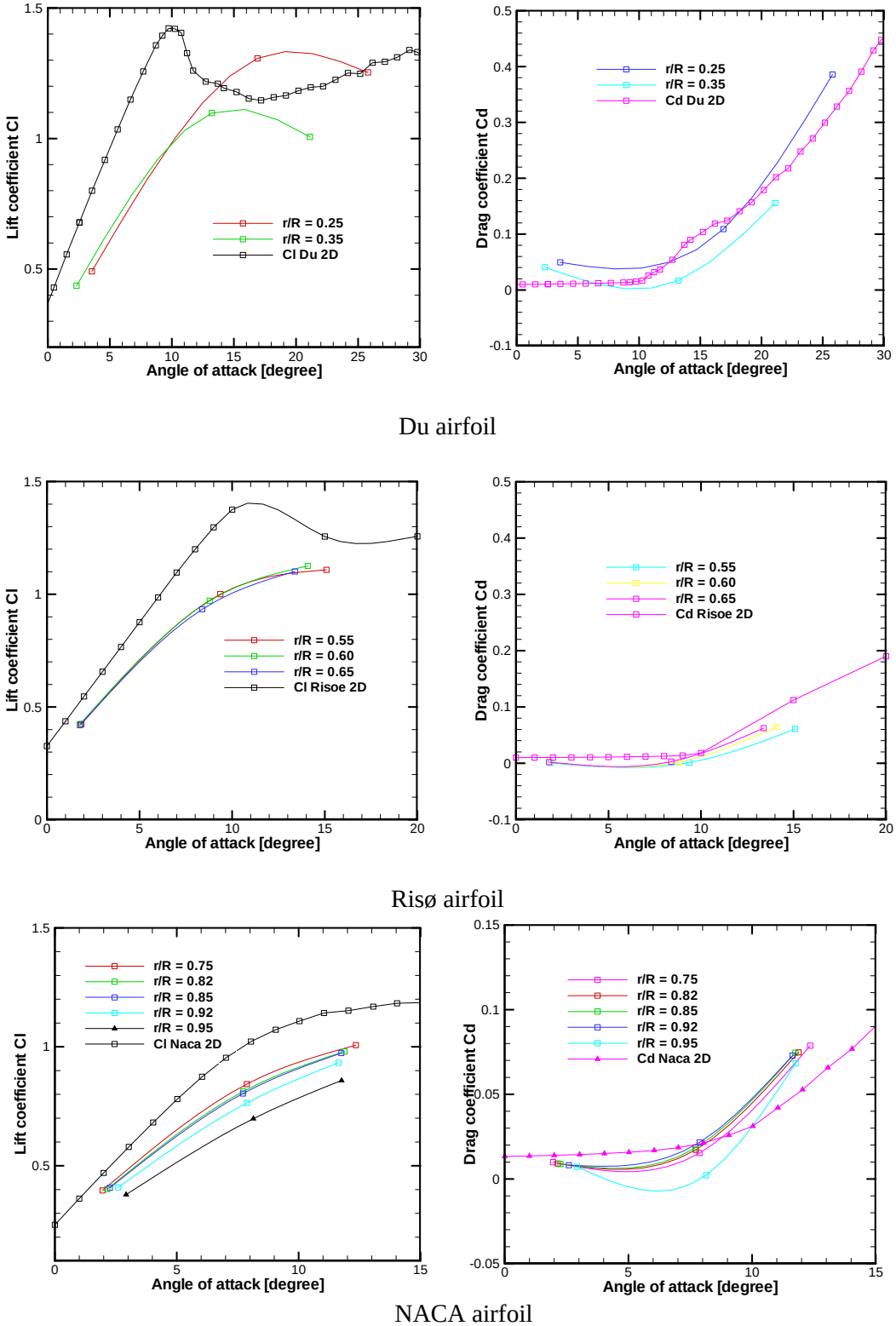

Fig.9. Airfoil characteristics of three airfoils extracted from CFD

5 Check on the extracted airfoil data using a BEM code

The BEM method is the most popular technique for computing loads and power of wind turbines. The method is a one-dimensional approach based on the actuator disc principle that corresponds to a rotor with an infinite number of blades. To account for the difference in circulation between an N-bladed rotor and an actuator disc, a tip loss factor was derived by Prandtl and introduced in the BEM technique by Glauert. In Glauert's method a correction factor, *F*, is introduced as follows,

$$F = \frac{2}{\pi}\cos^{-1}[\exp(-\frac{B(R-r)}{2r\sin\phi})], \tag{3}$$

where *B* denotes the number of blades and *(R-r)* is the distance from the tip to the local radial cross-section. Different tip loss correction models have been developed to calculate load and power of wind turbines. Shen *et al.* [9] analyzed a few existing tip loss correction models and found inconsistencies in the existing correction models, which results in incorrect predictions of the aerodynamic behaviour in the proximity of the tip. To remedy the inconsistencies, a new tip loss correction model was proposed:

$$F_1 = \frac{2}{\pi}\cos^{-1}[\exp(-g\frac{B(R-r)}{2r\sin\phi})], \tag{4}$$

Where
$$g = \exp[-0.125(B\lambda - 21)] + 0.1, \tag{5}$$

Where, λ is the tip speed ratio.

In order to validate the technique of determination of angle of attack, the obtained 10 sectional airfoil data are put into the BEM code without further correction. The same three cases where computation data were used for extracting airfoil data are first investigated. In Figure 10, the reproduced normal force distribution from the BEM with the derived airfoil data is compared with the original experimental data and BEM code using the Shen's tip loss correction model with 2D airfoil data. From the figure, the trend is consistent and small differences are seen at the blade root at the wind speed of 24 m/s. This is mainly due to the flow separation. It is worth noting that the load from BEM with 2D airfoil data is not smooth because the blade is consisted of different airfoils.

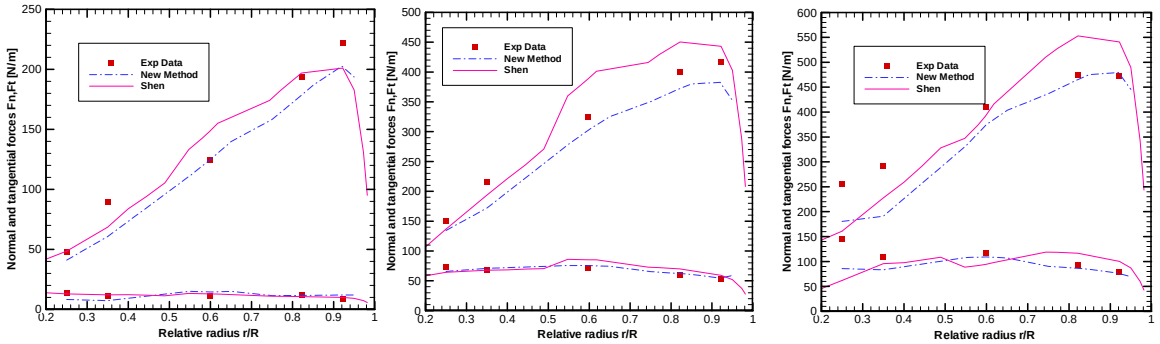

v_{tun} = 10 m/s v_{tun} = 15 m/s v_{tun} = 24 m/s

Fig. 10: Force distributions from experimental data, BEM using derived airfoil data and BEM using Shen's tip loss corrections for the MEXICO rotor at rotation speed of 424 rpm and a pitch angle of 0.7°.

To check whether the obtained airfoil characteristics can be used to predict the performance of the MEXICO rotor at other operating conditions, different tunnel speeds, pitch angles and rotor speeds are selected. Figure 11 show the axial and tangential forces at a rotor speed about of 424 rpm, different pitch angles and tunnel wind speeds. From the figure, very good agreements between the BEM code with extracted airfoil data and the experimental data are seen for both axial and tangential forces.

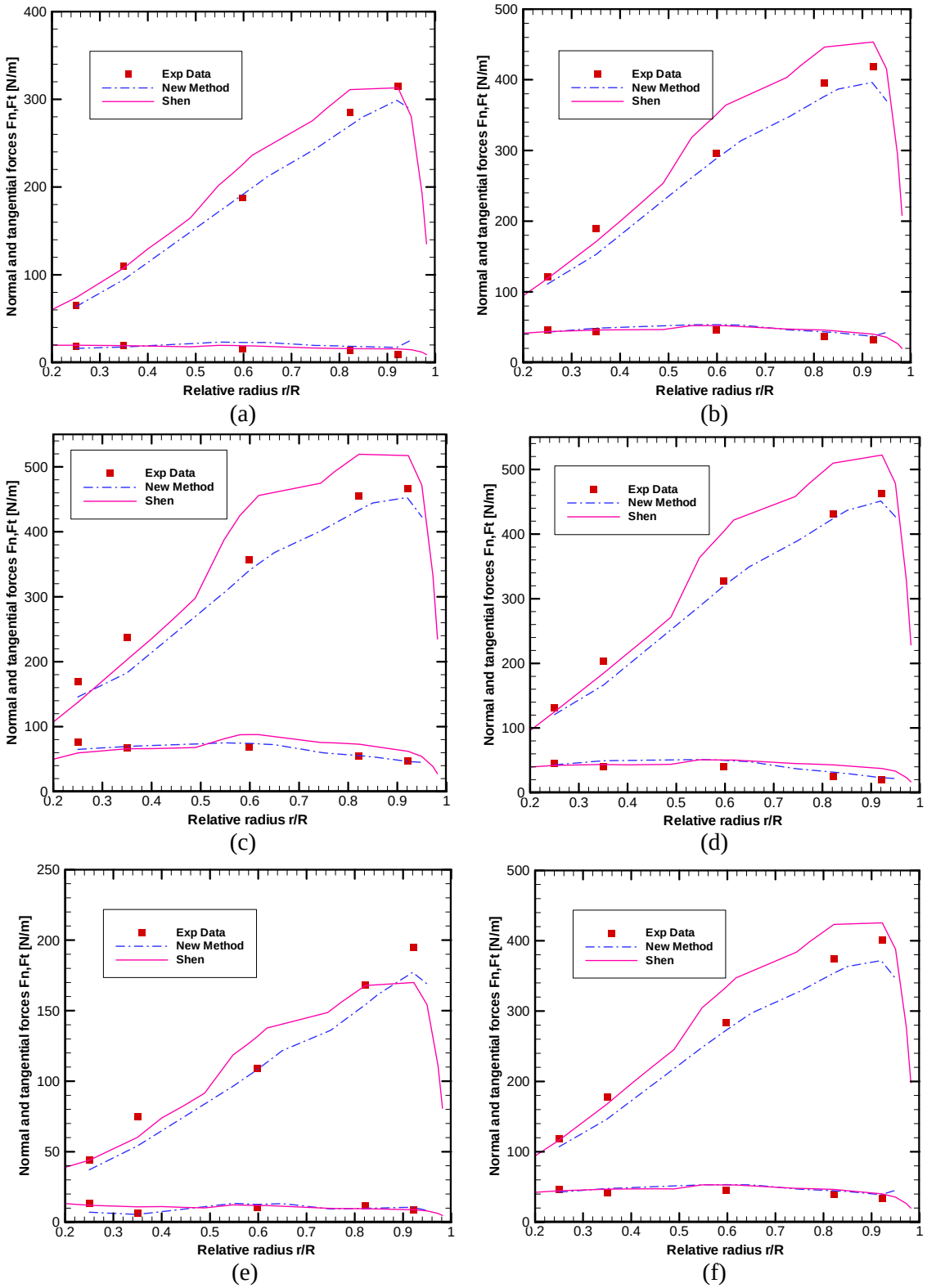

Fig. 11. Comparison of force distributions from experimental data and BEM using the derived airfoil data for the MEXICO rotor at rotation speed of 424.0 rpm.

(a) V_{tun}=11 m/s, θ_p=-2.3°; (b) V_{tun}=14.93 m/s, θ_p=-2.3°; (c) V_{tun}=18 m/s, θ_p=-2.3°;
(d) V_{tun}=14.91 m/s, θ_p= -5.3°; (e) V_{tun}=10 m/s, θ_p=1. 7°; (f) V_{tun}=15 m/s, θ_p=-1.3°;

6 Conclusions

In the present paper, the flow fields of the MEXICO rotor under three axial flow conditions are simulated by CFD with *k-ω* SST turbulence model. The local airfoil characteristics were derived from CFD computations using the azimuthally averaged velocity and the forces on the blade to extract lift and drag coefficients, C_l and C_d. The sectional airfoil data are fitted using spline interpolation functions and they are very different from the 2D airfoil data. The derived airfoil data are loaded into a BEM code without any correction model and checked by comparing the axial and tangential forces on the blade with experiments at the same operational conditions. Although the azimuthally averaged velocity is not exactly identical to the local velocity used for defining the angle of attack, there was a good agreement between the mechanical power predicted by BEM and experiment results. Because of the flow separation, the recalculated forces are lower than the experiment value near the root span at the wind speed of 24 m/s. The results from BEM with Shen's tip loss correction are also presented, and the calculated forces change suddenly on mid span. The reason may be that the MEXICO rotor constructed with three geometrically different airfoils. The derived airfoil data are also used to calculate the forces under the conditions of other pitch angles and tunnel wind speeds. Good agreements are also obtained in these results when compared with the measurements.

Acknowledgments

This paper is supported by Funds of International S&T Cooperation Program of China (Grant No. 2010DFA64660), the National Natural Science Foundation of China (Grant No. 50706041) and Danish Council for Strategic Research (Grant No. 12-130590).

REFERENCES

[1] HANSEN M O L, SØRENSEN J N, VOUTSINAS S, et al. "State of the art in wind turbine aerodynamics and aeroelasticity". *Progress in Aerospace Sciences*, 2006,42(4): 285-330.

[2] Snel H, Houwink R, Piers WJ, van Bussel GJW, Bruining A. "Sectional prediction of 3-D effects for stalled flow on rotating blades and comparison with measurements". *EWEC 1993*; 395-399.

[3] Du Z, Selig M. "A 3-D stall-delay model for horizontal axis wind turbine performance predictions". *AIAA-98-0021*, 1988.

[4] Chaviaropoulos PK, Hansen MOL. "Investigating three-dimensional and rotational effects on wind turbine blades by means of a quasi-3D Navier-Stokes solver". *Journal of Fluids Engineering 2000*, 122: 330-336.

[5] H Yang, WZ Shen, JN Sørensen, WJ Zhu, "Extraction of airfoil data using PIV and pressure measurements". *Wind Energy*, 2011, 14 (4): 539-556, DOI: 10.1002/we.441.

[6] JOHANSEN J and SØRENSEN N N. "Aerofoil characteristics from 3D CFD rotor computations". *Wind Energy*, 2004, 7(4): 283-294.

[7] SCHEPERS J G and SNEL H. "Model experiments in controlled conditions". *ECN Report*, ECN-E-07-042, 2007.

[8] Per-Åge Krogstad, Pål Egil Eriksen. "Blind test" calculations of the performance and wake development for a model wind turbine. Renewable Energy, 2013, 50: 325-333.

[9] SHEN W Z, MIKKELSEN R, SØRENSEN J N, et al. "Tip loss corrections for wind turbine computations". *Wind Energy*, 2005, 8(4): 457-475.